.

Shell-model studies of the astrophysical rp-process reactions ^{34}S(p,γ)^{35}Cl and ^{34g,m}Cl(p,γ)^{35}Ar

W. A. Richter[1,2], B. A. Brown[3], R. Longland[4], C. Wrede[3], P. Denissenkov[5,6], F. Herwig[5,6], D. Kurtulgil[5,7], M. Pignatari[5,8,9,10], and R. Reifarth[5,7]

[1] *University of Stellenbosch, South Africa*

[2] *iThemba LABS, Somerset West, South Africa**

[3] *Department of Physics and Astronomy and National Superconducting Cyclotron Laboratory, Michigan State University, East Lansing, Michigan 48824-1321, USA* †

[4] *Department of Physics, North Carolina State University, Raleigh, North Carolina, 27695, USA*

[5] *NuGrid Collaboration*

[6] *Department of Physics and Astronomy, University of Victoria, Victoria, Canada*

[7] *Goethe University, Max-von-Laue-Str. 1, Frankfurt am Main, 60438, Germany*

[8] *E.A. Milne Center for Astrophysics, Department of Physics & Mathematics, University of Hull, HU6 7RX, United Kingdom.*

[9] *Konkoly Observatory, Research Center for Astronomy and Earth Sciences, Hungarian Academy of Sciences, Konkoly Thege Miklos ut 15-17, H-1121 Budapest, Hungary. and*

[10] *Joint Institute for Nuclear Astrophysics - Center for the Evolution of the Elements, USA*

Background: Dust grains condensed in the outflows of pre-solar classical novae should have been present in the proto-solar nebula. Candidates for such pre-solar nova grains have been found in primitive meteorites and can in principle be identified by their isotopic ratios, but the ratios predicted by state-of-the-art 1D hydrodynamic models are uncertain due to nuclear-physics uncertainties.

Purpose: To theoretically calculate the thermonuclear rates and uncertainties of the ^{34}S(p,γ)^{35}Cl and ^{34g,m}Cl(p,γ)^{35}Ar reactions and investigate their impacts on the predicted ^{34}S/^{32}S isotopic ratio for pre-solar nova grains.

Method: A shell-model approach in a (0+1) $\hbar\omega$ model space was used to calculate the properties of resonances in the ^{34}S(p,γ)^{35}Cl and ^{34g,m}Cl(p,γ)^{35}Ar reactions and their thermonuclear rates. Uncertainties were estimated using a Monte-Carlo method. The implications of these rates and their uncertainties on sulfur isotopic nova yields were investigated using a post-processing nucleosynthesis code. The rates for transitions from the ground state of ^{34}Cl as well as from the isomeric first excited state of ^{34}Cl were explicitly calculated.

Results: At energies in the resonance region near the proton-emission threshold many negative-parity states appear. Energies, spectroscopic factors and proton-decay widths are reported. The resulting thermonuclear rates are compared with previous determinations.

Conclusions: The shell-model calculations alone are sufficient to constrain the variation of the ^{34}S/^{32}S ratios to within about 30%. Uncertainties associated with other reactions must also be considered, but in general we find that the ^{34}S/^{32}S ratios are not a robust diagnostic to clearly identify presolar grains made from nova ejecta.

PACS numbers: 26.30.-k,21.60.Cs,27.30.+t

*Electronic address: richter.werner@gmail.com

†Electronic address: brown@nscl.msu.edu

I. INTRODUCTION

A classical nova is a thermonuclear explosion on the surface of a white dwarf star accreting hydrogen-rich gas from a companion star in a binary system. In cooling nova outflows, material that has undergone nucleosynthesis can condense to form dust grains. Such grains should have been present in the proto-solar nebula and can be searched for in primitive meteorites and, in principle, identified by their isotopic ratios. Indeed, several candidate pre-solar nova grains have been recovered but their identifications are often ambiguous due to uncertainties associated with the thermonuclear reaction rates in novae.

For example, the ^{34}S/^{32}S ratio has the potential to aid in pre-solar novae grain classification, but the nuclear reaction rate uncertainties are too large for it to be an unambiguous tool [1]. ^{34}S can be destroyed in novae through the ^{34}S(p,γ)^{35}Cl reaction or bypassed by the ^{34}Cl(p,γ)^{35}Ar reaction if the rate is fast enough to dominate the beta decay rate ^{34}Cl $\rightarrow$ ^{34}S ($T_{1/2} = 1.53$ s for the ground state). The thermonuclear rates of these reactions are unknown at nova temperatures due to a lack of experimental nuclear physics data for the resonances up to about 800 keV above the ^{35}Ar proton separation energy [2]. Moreover, some nova models treat the ^{33}S(p,γ)^{34}Cl and ^{34}Cl(p,γ)^{35}Ar rates as total rates, without separately considering the ground state ^{34g}Cl and the isomeric first excited state ^{34m}Cl (Ex = 0.146 keV, $T_{1/2} = 2.5$ min). However, similar to the case of ^{26}Al, the ^{34}Cl ground state and its long-lived isomer are not necessarily in thermal equilibrium at nova temperatures and it is therefore necessary to calculate the reaction rates on both initial states, in order to represent their influence accurately in a nucleosynthesis calculation [3], [4], [5], and in some cases capture on an excited state can dominate a thermonuclear reaction rate even when it is in thermal equilibrium with the ground state [6]. Therefore it is important to constrain not only the ^{34g}Cl(p,γ)^{35}Ar reaction rate, but also the ^{34m}Cl(p,γ)^{35}Ar rate.

In a recent experiment [7] the ^{34}S(^{3}He,d)^{35}Cl reaction was studied and proton-transfer spectroscopic factors measured for 21 states in an excitation energy region of one MeV above the ^{34}S(p,γ) threshold energy ($S_p = 6.371$ MeV). The experimental cross sections are proportional to $C^2S^+ = [(2J_f+1)/(2J_i+1)]\ C^2S$ ($J_i = 0$ in this case), the same quantity that enters the reaction rate. It is not necessary to determine the J_f values of the resonances explicitly. These results were considered in Ref. [8] to obtain the ^{34}S(p,γ)^{35}Cl reaction rate. We will compare our calculations with these results.

In a study by Fry *et al.* seventeen [2] new ^{35}Ar levels have been detected in the energy region $E_x = 5.9 - 6.7$ MeV and their excitation energies have been determined, but not spins, parities, widths, or branching ratios. Because of the paucity of such information it is not yet possible to derive meaningful experimental ^{34g,m}Cl(p,γ)^{35}Ar reaction rates.

Estimates based on shell-model calculations are complicated by high level density and the presence of negative-parity states in the resonance region near the proton-emission threshold. To address this problem, we present calculations of ^{35}Cl+p and ^{35}Ar+p resonances in a (0+1) $\hbar\omega$ basis with the code NuShellX [9] to provide energies, spectroscopic factors and proton-decay widths. Such calculations were carried out recently for the first time for the ^{30}P(p,γ)^{31}S reaction [10].

We use the shell-model results to calculate the thermonuclear rates for radiative proton capture reactions on the ground states of ^{34}S and ^{34}Cl, and on the isomeric first-excited state of ^{34}Cl. Uncertainties for the total calculated reaction rates have been included based on Monte-Carlo techniques [11]. The implications of the new rates on the predicted ^{34}S/^{32}S ratio in pre-solar nova grains have been investigated using a post-processing nova nucleosynthesis code.

The results given in this paper supersede those given in the preliminary conference series publication [12].

II. THE SHELL-MODEL CALCULATIONS

For positive-parity states we use the $(1s_{1/2}, 0d_{5/2}, 0d_{3/2})$ (sd) model space with the USDB Hamiltonian [13]. For negative-parity states the model space is extended to include $1\hbar\omega$ excitations. This involves one-nucleon excited from from the p shell $(0p_{3/2}, 0p_{1/2})$ shell to the sd shell, or one nucleon excited from the sd to the pf shell $(1p_{1/2}, 1p_{3/2}, 0f_{7/2}, 0f_{5/2})$. The spurious states for these $1\hbar\omega$ negative-parity states were removed using the Gloeckner-Lawson method [14]. For $1\hbar\omega$ we start with WBP Hamiltonian from [15]. The sd part of WBP was based on the older USD Hamiltonian [16]. We have replaced that part with the USDB Hamiltonian. The wavefunctions for $1\hbar\omega$ negative-parity states in the nuclei we consider are dominated by the sd to pf excitations. That part of the WBP Hamiltonian is based on the WBMB Hamiltonian obtained for the $sd - pf$ model space in [17]. For our purpose, the single-particle energies for $1p_{1/2}, 1p_{3/2}$, and $0f_{7/2}$ were adjusted to reproduce the energies of the strongest states observed in the one-nucleon transfer reactions from ^{34}S to ^{35}S and ^{35}Cl. The spin-orbit splitting for $0f_{7/2}$-$0f_{5/2}$ was set to 6 MeV.

The effective operators for M1 and E2 gamma decay are taken from [18]. We use the free-nucleon operator for E1 gamma decay. But we note that all of the reaction rates considered here are dominated by the proton-decay width, and thus the uncertainty in the rates coming from the gamma decay rates is negligible.

For the (p, γ) reactions the most important aspects of the calculation are the energies and the one-nucleon spectroscopic factors. The best data for this comparison is the one-nucleon transfer data from ^{34}S to ^{35}Cl. The experi-

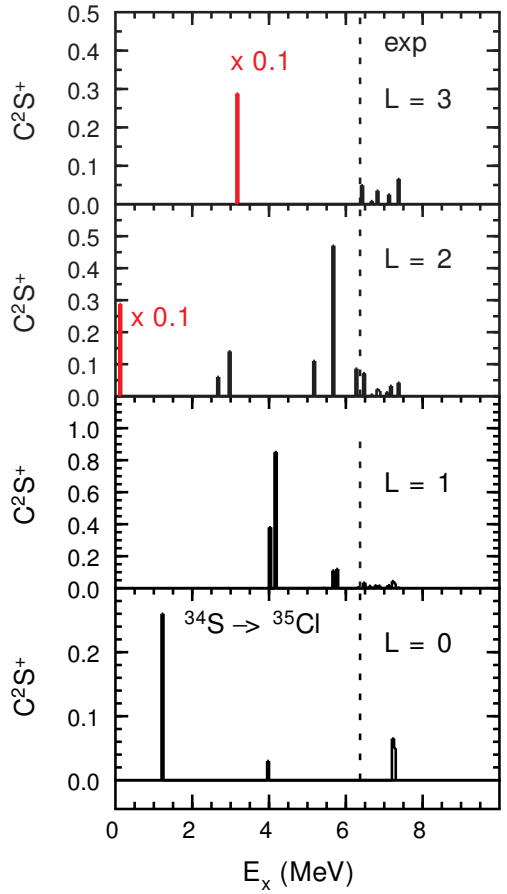

FIG. 1: Experimental spectroscopic factors, $C^2S^+ = (2J_f+1)$ C^2S, for single-proton transfer on the target ^{34}S. The results below 5.8 MeV are from Ref [19], and the results from 6.2 to 7.4 MeV are from [7]. The dotted line shows the value of the proton separation energy.

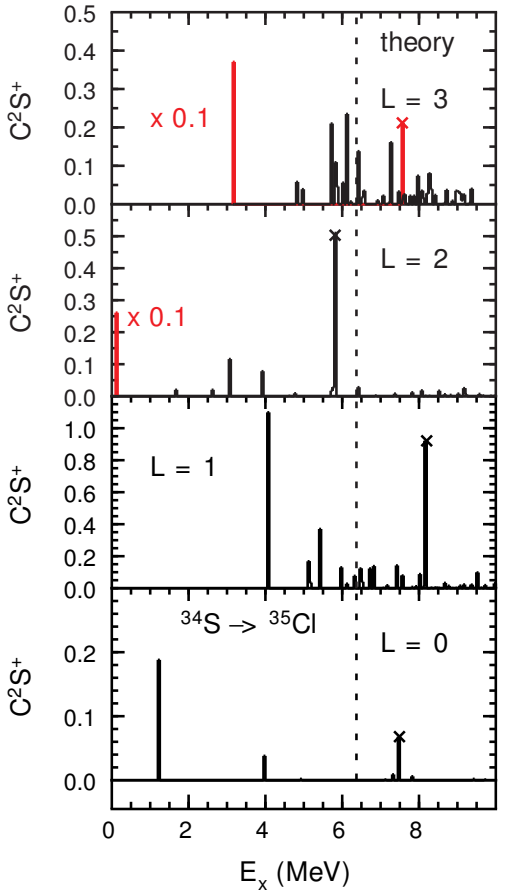

FIG. 2: Theoretical spectroscopic factors, $C^2S^+ = (2J_f+1)$ C^2S, for single-proton transfer on the target ^{34}S. The states with $T = 3/2$ are indicated by a cross on top. The dotted line shows the value of the proton separation energy.

mental spectroscopic factors, $C^2S^+ = (2J_f+1)$ C^2S, are shown in Fig. 1, and the theoretical results are shown in Fig. 2. The results for 16 states below 5.8 MeV are from [19], and the results for 21 states from 6.2 to 7.4 MeV are from Ref. [7]. The spectroscopic factors have not been measured between 5.8 and 6.2 MeV. Many of the states observed [7] are assigned $L = (0, 1)$. Our calculations indicate that there are many more states with $L = 1$ in this energy region compared to those with $L = 0$. For the purpose of comparison we show the spectroscopic factors for these as $L = 1$ in Fig. 1.

The results for positive parity states based on the USDB Hamiltonian are in good agreement with experiment. The relatively strong $L = 2$ state near 5.7 MeV is the $T = 3/2$ isobaric analogue of the ^{35}S $3/2^+$ ground state. The relatively strong $L = 0$ state near 7.2 MeV is the $T = 3/2$ isobaric analogue of the ^{35}S $1/2^+$ first excited state.

The results for negative parity states are in reasonable agreement with experiment. The results from Ref. [7] do not have unique L values or J_f assignments, and we are not able to make a state by state comparison. Between 6.2 and 7.4 MeV 21 states are observed experimentally [7] compared to 40 states with $J^\pi_f = 1/2^+, 3/2^+, 5/2^+$, $1/2^-$, $3/2^-$, $5/2^-$ and $7/2^-$ calculated. Many of these states may have not been observed due to their very small spectroscopic factors. The strong $L = 3$ states near 5.9 MeV are in the energy window of 5.8 to 6.2 MeV not covered by experiment. The strong $L = 3$ state near 7.3 MeV is the $T = 3/2$ isobaric analogue of the ^{35}S $7/2^-$ third excited state. The relatively strong $L = 1$ state near 8.2 MeV is the $T = 3/2$ isobaric analogue of the ^{35}S $3/2^-$ fourth excited state.

The strongest $L = 1$ state at 4.1 MeV is $3/2^-$. In experiment this strength gets split over two nearby $3/2^-$ states separated by 118 keV. The second $3/2^-$ state cannot be reproduced by the calculation. This is a potential problem with the calculation. But it may be $3\hbar\omega$ related to a ^{32}S plus $(fp)^3$ cluster-type structure. This could explain the near degeneracy of two states with the same J^π. These $3\hbar\omega$ configurations would not directly con-

tribute to the one-nucleon spectroscopic strengths, but they would introduce more states in the spectrum and cause the spectroscopic strength to be split over nearby states as is the case with these $3/2^-$ states.

We consider the reactions ^{34}S(0^+)(p,γ)^{35}Cl and ^{34g}Cl(0^+) (p,γ)^{35}Ar. The initial states are isobaric analogues, and the final nuclei are mirrors of each other. The nuclear structure input is the same except that the spectroscopic factor to ^{35}Ar are reduced a factor of two compared to those to ^{35}Cl due to the difference in the C^2 factor. The energy shifts between the states in these mirror nuclei depend on the state and are on the order of a hundred keV or less.

We also consider the reaction rate for ^{34m}Cl(3^+) (p,γ)^{35}Cl from the isomeric state at 146 keV in ^{34}Cl. All three of these reactions depend on the properties of states in the region of 6-7 Mev in ^{35}Cl and ^{35}Ar.

In the ^{36}Ar(d,t)^{35}Ar reaction [2], 22 levels were observed between 5.9 and 6.7 MeV in ^{35}Ar. Our shell-model results have 19 levels in this region of excitation energy. In [7] and [8] 15 levels with $J < 5/2$ are observed between 6.3 and 7.0 MeV in ^{35}Cl. Our shell-model results have 14 levels with $J < 5/2$ in this region of excitation energy. Given the high level density this is good agreement between theory and experiment.

III. RESULTS FOR THE REACTION RATES

We follow the standard procedures used to obtain reaction rates [11]. The shell-model calculations provide the spectroscopic factors and gamma decay widths, Γ_γ. The proton decay width is obtained from $\Gamma_p = C^2S\Gamma_{sp}$ where Γ_{sp} is the single-particle proton decay based on the proton scattering from a Woods-Saxon potential [20]. These are then combined to obtain the $\omega\gamma$ and the reaction rates.

The contributions from $L = 0, 1$ are about an order of magnitude larger than those with $L = 2, 3$ due to the larger centrifugal barriers for the high L. The spectroscopic factors for $L = 0, 1$ in the excitation energy region of interest for our reaction rates are shown in Fig. 3. The details for the theoretical input to the reaction rates for $L = 0, 1$ are given in Tables I, II and III. The reaction rates are shown in Figs. 4, 5, and 6. The bottom part of these figures show the percentage contribution from each final state. The most important states are labeled by the state numbers shown in Fig. 3 and the Tables.

We obtained uncertainties for the reaction rates based on Monte Carlo techniques [11]. The results for the quartiles of the cumulative reaction rate distribution are shown in Fig. 4. We assume 200 keV uncertainty for the resonance energy, and factor of two uncertainties for the gamma-decay and proton-decay widths. The error in the rate from the gamma-decay width is negligible since, as shown in the Tables, the proton-decay width is much smaller than the gamma-decay for those states in the excitation energy region that contribute to the rate.

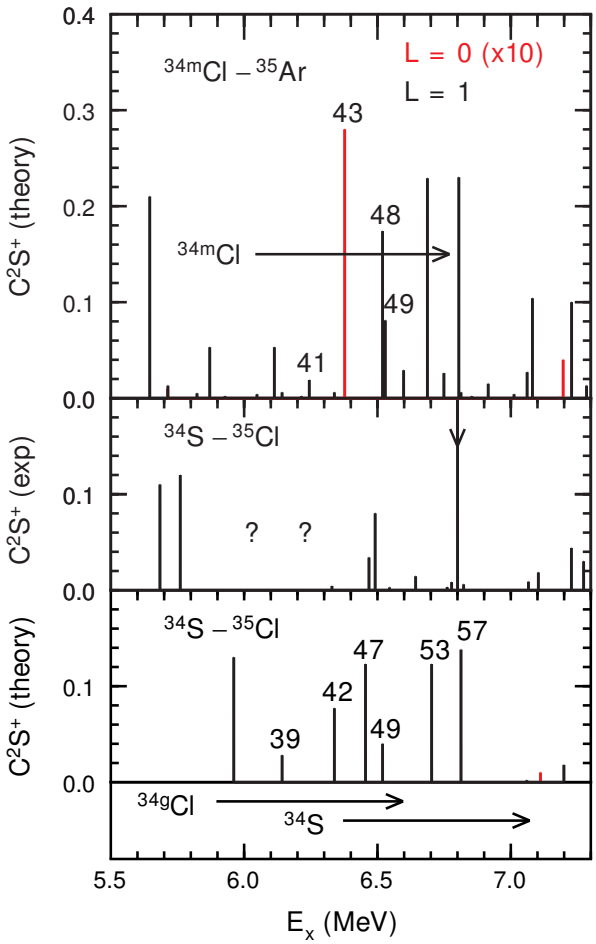

FIG. 3: Spectroscopic factors, C^2S+, for $L = 0, 1$ in the excitation energy region of importance for the reactions rates. For a given spectroscopic factor, $L = 0$ is about a factor of 10 stronger than $L = 1$ in the reaction rate due to the smaller centrifugal barrier. For this reason the values for $L = 0$ have been multiplied by 10 to show their relative importance to $L = 1$. The bottom panel shows the theoretical values for ^{34}S to ^{35}Cl. The peaks are labeled by their order in the excitation energy spectrum. The middle panel shows the experiment values from Ref. [19] for $E_x < 5.8$ MeV and from Refs. [7] and [8] for $E_x > 6.3$ MeV. Experimental results are not known for the region between 5.8 and 6.3 MeV. The line at 6.8 MeV labeled by a down arrow is given in [8] by $C^2S+ < 4$. The arrows at the bottom show the range of excitation energy important for the ^{34}S(p,γ)^{35}Cl reaction starting at $S_p = 6.371$ MeV, and the ^{34g}Cl(p,γ)^{35}Ar starting at $S_p = 5.896$ MeV in the mirror nucleus ^{35}Ar. The theoretical spectroscopic factors for ^{34g}Cl(p,γ)^{35}Ar exactly are a factor of two smaller than those shown for ^{34}S(p,γ)^{35}Cl due to the difference in the C^2 factors. The upper panel shows the spectroscopic factors for ^{34m}Cl(3^+)(p,γ)^{35}Ar. The arrow starting at $S_p = 6.042$ MeV shows the range of excitation energy of importance for that reaction. These spectroscopic factors lead to a reaction rate for ^{34m}Cl(3^+)(p,γ)^{35}Ar that is about a factor of four larger than that for ^{34g}Cl(0^+)(p,γ)^{35}Ar in the region at T9=0.2 (GigaK).

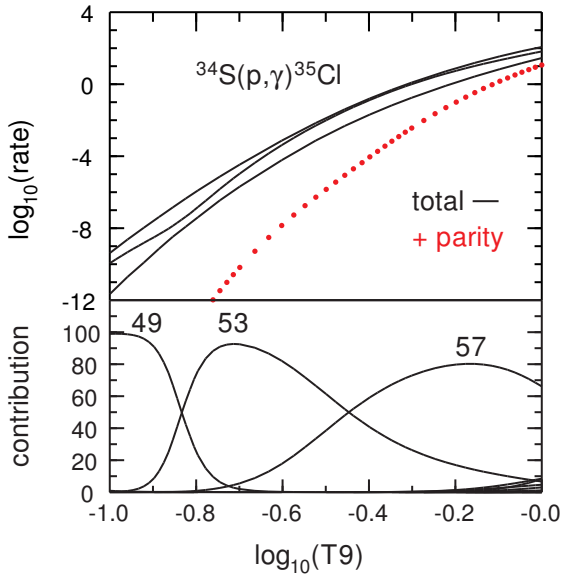

FIG. 4: Top panel: The calculated reaction rate for ^{34}S(p,γ)^{35}Cl versus temperature T9 (GigaK). The upper and lower black lines show the low-rate and the high-rate obtained from the Monte-Carlo calculations. The middle black line shows the rate obtained directly from the input in Table I. The results from positive parity states only are shown by the red dots. Bottom panel: The contribution of individual resonances in Table I.

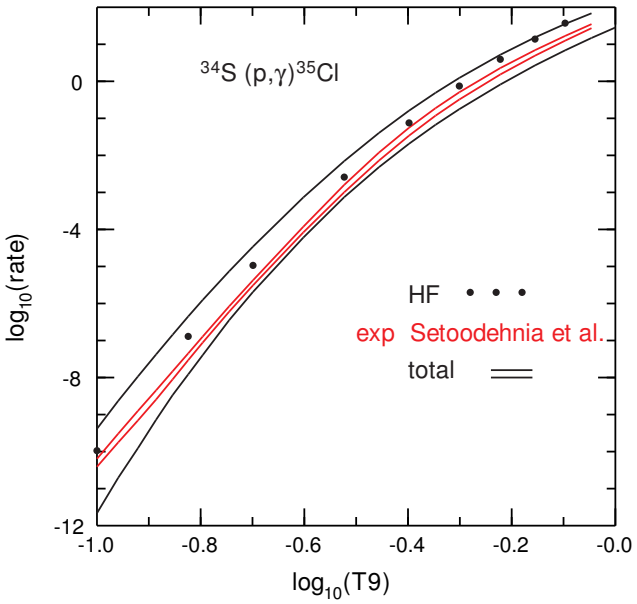

FIG. 5: The calculated reaction rates for ^{34}S(p,γ)^{35}Cl compared with the rate rate [8] based on experimental data from [7] and the Hauser-Feshbach rate from Ref. [21].

In Fig. 5 our results for ^{34}S(p,γ)^{35}Cl are compared with the rate [8] based on experimental data from [7]. The Hauser-Feshbach rate from Ref. [21] is also shown. All of these are in relatively good agreement. This comparison with experiment indicates that our assumed uncertainties are reasonable.

Results for the $L = 0, 1$ spectroscopic factors and gamma-decay widths are given in Tables II and III. These were used to obtain the proton-decay widths $\omega\gamma$ values given in Table II and III.

The top panel of Fig. 6 shows the total reaction rate versus temperature T9 (GigaK) for ^{34g}Cl(p,γ)^{35}Ar from the 0^+ ground state of ^{34}Cl. The bottom panel shows the contribution from individual resonances given in Table II. The spectroscopic factors for the states in Table II are half of those in Table I for ^{34}S due the difference in the C^2 factor.

The top panel of Fig. 7 shows the total reaction rate versus temperature T9 (GigaK) for ^{34m}Cl(p,γ)^{35}Ar from the 3^+ isomeric state of ^{34}Cl at 0.146 MeV. The bottom panel shows the contribution from individual resonances given in Table III. The rate is dominated by an $L = 0$ transition to a $7/2^+$ state.

The increase in the reaction rate due to thermal population of an excited state is referred to as a stellar enhancement factor (SEF). In the case of ^{34}Cl the reaction rate from the isomeric state is much larger than from the ground state leading to a large SEF. The previous

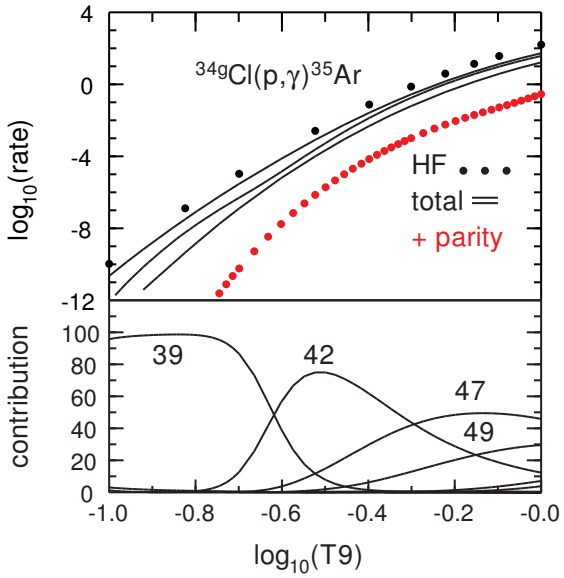

FIG. 6: Top panel: The calculated reaction rates for ^{34g}Cl(p,γ)^{35}Ar versus temperature T9 (GigaK). The upper and lower black lines show the low-rate and the high-rate obtained from the Monte-Carlo calculations. The middle black line shows the rate obtained directly from the input in Table II. The results from positive parity states only are shown by the red dots. The results are compared to the Hauser-Feshbach rate from Ref. [21]. Bottom panel: The contribution of individual resonances in Table II.

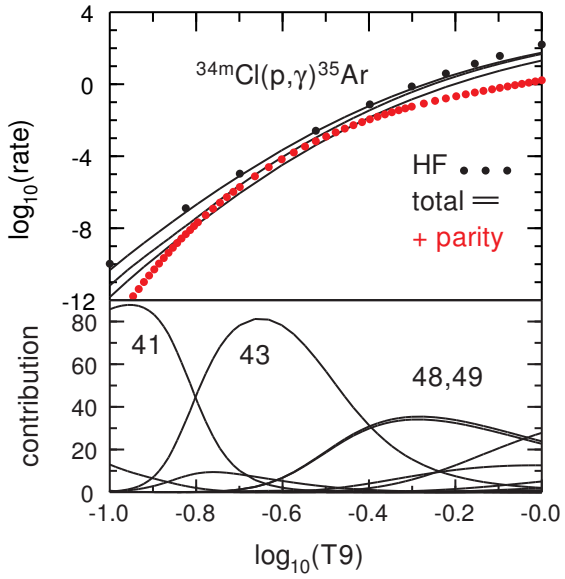

FIG. 7: Top panel: The calculated reaction rates for ^{34m}Cl(p,γ)^{35}Ar versus temperature T9 (GigaK). The upper and lower black lines show the low-rate and the high-rate obtained from the Monte-Carlo calculations. The middle black line shows the rate obtained directly from the input in Table III. The results from positive parity states only are shown by the red dots. The results are compared to the Hauser-Feshbach rate from Ref. [21]. Bottom panel: The contribution of individual resonances in Table III.

calculation reported for ^{34g,m}Cl [22] is only based on the *sd*-shell results for positive-parity states resulting in rates that are much smaller than those obtained here with the inclusion of the negative-parity states.

IV. NUCLEOSYNTHESIS SIMULATIONS

The astrophysical implications of the present shell-model calculations were investigated using the Nova Framework [23], which combines the stellar evolution code MESA with the post-processing nucleosynthesis tools of NuGrid. An ONe white dwarf of 1.3 solar masses and an initial luminosity of $\log(L/L_\odot) = -2.52$ was assumed along with a mass accretion rate of 2×10^{-10} solar masses per year, where the accreted material consisted of 50% solar and 50% ONe white-dwarf compositions. For the latter, we used the "Barcelona" ONe white-dwarf composition (see Fig. 4 in Ref. [23]). Using these parameters the chemical composition of the nova ejecta is close to that of model ONe6 of Ref. [24] (see Fig. 11 in Ref. [23]). The maximum temperature of H burning in our model reaches 355 MK. The thermonuclear rates employed were initially identical to those used in Ref. [23], except we adopted the relatively new and improved ^{33}S(p,γ)^{34}Cl reaction rate from Parikh *et al.* [25], and the ^{34}S(p,γ)^{35}Cl, ^{34g}Cl(p,γ)^{35}Ar, and ^{34m}Cl(p,γ)^{35}Ar reactions were adopted from the present work. Thermal communication between the ground and metastable states of ^{34}Cl through all low-lying ^{34}Cl states was implemented [26]. Using the median rates under these assumptions, we find the ^{34}S/^{32}S mass-fraction ratio for nova ejecta to be 0.049. When the ^{34g}Cl(p,γ)^{35}Ar and ^{34m}Cl(p,γ)^{35}Ar rates are varied together within their uncertainties, the ratio barely changes. When the ^{34}S(p,γ)^{35}Cl rate is varied within its uncertainties, the ratio varies from 0.044 to 0.057. Varying all three reaction rates together leads to the most extreme range of 0.043 to 0.057.

Evidently, the nuclear physics uncertainties calculated for the reactions considered in the present shell-model calculations have only a moderate impact on the uncertainties associated with this isotopic ratio. Despite the large uncertainties associated with the individual resonance energies, the density of states is high enough that the resonances tend to compensate for each other statistically. The resulting variations in the thermonuclear reaction rates are not large enough to cause dramatic variations in this isotopic ratio.

The sulfur ratios presented above are centered near the solar value of 0.047 and are indistinguishable from the range of isotopic ratios predicted from CCSN models. For instance, using models by [7] and [27] estimated a ^{34}S/^{32}S ratio for CCSN models in the range of 0.026 and 0.053. However, the observed 34S/32S ratio from presolar SiC grains of Type X and Type C condensed in CCSNe ejecta range between 0.003 and 0.036. The lowest observed ratio is comparable to a basically pure ^{32}S composition, that is not reached in any part of the CCSN ejecta according to stellar simulations [28]. This discrepancy was solved by considering the contribution of ^{32}Si in C-rich He-shell ejecta: ^{32}Si has an half-life of 172 years and is condensing as Si in SiC grains, much more efficiently than S [29]. This will produce an anomalous low ^{34}S/^{32}S ratio in the presolar grain, mainly due to the Si/S fractionation. Fujiya et al. [30] analyzed the isotopic ratios of S in presolar SiC of Type AB, which among many different stellar sources could also be made in CCSNe ejecta [31]. In these types of grains, the range of measured ^{34}S/^{32}S is going between 0.027 and slightly higher than solar.

In summary, the ^{34}S/^{32}S ratio measured in presolar grains made in CCSNe is extremely large once the ^{32}Si radiogenic contribution to ^{32}S and the Si/S fractionation are taken into account, covering also the typical values obtained from Novae simulations.

This unfortunate conclusion is different from the conclusion of Ref. [7] where a distinct range of 0.014 to 0.017 was derived for the nova grains based on indirect measurements of the ^{34}S(p,γ)^{35}Cl reaction rate and the code SHIVA. A recent study by Setoodehnia *et al.* [8] suggests that the experimental ^{34}S(p,γ)^{35}Cl reaction-rate uncertainties reported in Ref. [7] may have been underestimated. However, the present ^{34}S(p,γ)^{35}Cl rates agree with those reported in Ref. [7] and therefore the discrepancy must lie elsewhere. We notice that when

we repeated the network-calculation procedure above using older rates [21], [32] for the ^{33}S(p,γ)^{34}Cl reaction, we found isotopic ratios in the range of 0.024 to 0.034, which are closer to those reported in Ref. [7]. Similarly, the ^{30}P(p,γ)^{31}S reaction rate can strongly influence the production of ^{34}S and other nuclides in novae [33] and is still essentially unknown experimentally despite a variety of dedicated efforts over the past 15 years [34]. It may be the case that different assumptions about the rates of these other reactions led to different resulting isotopic ratios. It is therefore important that all influential reaction rates are constrained.

V. CONCLUSIONS

In the comparison of our calculations for ^{34}S(p,γ)^{35}Cl with the recent experiment of Gillespie *et al.* and Setoodehnia *et al.* on ^{34}S(^{3}He,d)^{35}Cl there is generally good agreement between the calculated total rate and the experimental rate. Since ^{35}Ar is the mirror nucleus to ^{35}Cl, this gives us some confidence in the calculation of the ^{34g,m}Cl(p,γ)^{35}Ar rates.

The ^{34}S(p,γ)^{35}Cl and ^{34g,m}Cl(p,γ)^{35}Ar rates are all dominated by $L = 1$ transitions. The $L = 1$ are particularly strong for the ^{34m}Cl(p,γ)^{35}Ar reaction. The statistical Hauser-Feshbach rate differs from our total rate at lower temperatures but converges to our rate for higher temperatures. The calculations also identify the most prominent resonances in the reaction rates, and the analysis should serve as a guide for experiments as the spin-parity assignments of the most prominent resonances and their relative strengths are given.

The rates were implemented in a nova nucleosynthesis code including thermal population of the ^{34m}Cl isomer. Nucleosynthesis uncertainties associated with the shell-model calculations are not very large. We find that, in contrast to recent work, the ^{34}S/^{32}S isotopic ratio is not a strong discriminator of pre-solar grains of nova origin.

Acknowledgments This work is partly supported by NSF Grants PHY-1811855, PHY-1565546 and PHY-1913554, the Joint Institute for Nuclear Astrophysics NSF Grant PHY-1430152, and DOE grant DE-SC0016052. RL acknowledges support from U.S. Department of Energy, Grant No. DE-SC0017799 and Contract No. DE-FG02-97ER41041, WR acknowledges support from the University of Stellenbosch, South Africa. MP acknowledges significant support to NuGrid from STFC (through the University of Hull's Consolidated Grant ST/R000840/1), and access to VIPER, the University of Hull High Performance Computing Facility. MP acknowledges the support from the "Lendulet-2014" Program of the Hungarian Academy of Sciences (Hungary), and the ERC Consolidator Grant funding scheme (Project RADIOSTAR, G.A. n. 724560, Hungary).

[1] N. Liu, L. R. Nittler, C. M. O'D. Alexander, J. Wang, M. Pignatari, J. José, and A. Nguyen, The Astro. Jnl. **820**, 140 (2016)
[2] C. Fry, C. Wrede, S. Bishop, B. A. Brown, A. A. Chen, T. Faestermann, R. Hertenberger, A. Parikh, D. Pérez-Loureiro, H.-F. Wirth, A. García, and R. Ortez, Phys. Rev. C **91**, 015803 (2015)
[3] A. Coc, M. G. Porquet, and F. Nowacki, Phys. Rec. C **61**, 015801 (1999).
[4] P. Banerjee, G. W. Misch, S. K. Ghorui, and Y. Sun, Phys. Rev. C **97**, 065807 (2018).
[5] R. Reifarth, S. Fiebiger, K. Goebel, T. Heftrich, T. Kauch, C. Koeppchen, D. Kurtulgil, C. Langer, B. Thomas and M. Weigand, Int. Jour. Mod. Phys. A **33**, 1843011 (2018).
[6] H. Schatz, C. A. Bertulani, B. A. Brown, R. R. C. Clement, A. A. Sakharuk, and B. M. Sherrill, Phys. Rev. C **72**, 065804 (2005).
[7] S. A. Gillespie, A. Parikh, C. J. Barton, T. Faestermann, J. Jose, R Hertenberger, H.-F. Wirth, N. de Sereville, J. E. Riley, and M. Williams Phys. Rev. C **96**, 025801 (2017).
[8] K. Setoodehnia, J. H. Kelley, C. Marshall, F. Portillo Chaves and R. Longland, Phys. Rev. C **99**, 055812 (2019)
[9] B. A. Brown and W. D. M. Rae, Nuclear Data Sheets **120**, 115 (2014).
[10] B. A. Brown, W. A. Richter, and C. Wrede, Phys. Rev. C **89**, 062801(R) (2014)
[11] R. Longland, C. Iliadis, A. E. Champagne, J. R. Newton, C. Ugalde, A. Cocc, and R. Fitzgerald, Nucl. Phys. A **841**, 1 (2010)
[12] W. A. Richter and B. A. Brown, Journal of Physics Conference Series **966**, UNSP 012026 (2018).
[13] B. A. Brown and W. A. Richter, Phys. Rev. C **74**, 034315 (2006).
[14] D. H. Gloeckner and R. D. Lawson, Phys. Lett **B53**, 313 (1974).
[15] E. K. Warburton and B. A. Brown, Phys. Rev. C **46**, 923 (1992).
[16] B. A. Brown and B. H. Wildenthal, Ann. Rev. of Nucl. Part. Sci. 38, 29 (1988).
[17] E. K. Warburton, J. A. Becker and B. A. Brown, Phys. Rev. C **41**, 1147 (1990).
[18] W. A. Richter, S. Mkhize, and B. A. Brown, Phys. Rev. C 78, 064302 (2008).
[19] A. Graue, L. H. Herland, J. R. Lien, G. E. Sandvik, E. R. Cosman and W. H. Moore, Nucl. Phys. A **136**, 577 (1969)
[20] W. A. Richter, B. A. Brown, A. Signoracci and M. Wiescher, Phys. Rev. C 83, 065803 (2011).
[21] C. Iliadis, J. M. D'Auria, S. Starfield, W. J. Thompson, and M. Wiescher, Astrophys. J. Suppl. **134**, 151 (2001).
[22] J. Grineviciute, B. A. Brown, and H. Schatz, arXiv:1404.7268v1 (2014).
[23] P. A. Denissenkov, J. W. Truran, M. Pignatari, R. Trappitsch, C. Ritter, F. Herwig, U. Battino, K. Setoodehnia and B. Paxton, Mon. Not. R. Astron. Soc. **442**, 2058 (2014)

[24] J. José and M. Hernanz, Astrophys. J. **494** 680 (1998)
[25] A. Parikh, K. Wimmer, T. Faestermann, R. Hertenberger, J. José , H.-F. Wirth, C. Hinke, R. Krücken, D. Seiler, K. Steiger and K. Straub, Phys. Lett. B **737** 314 (2014)
[26] R. Reifarth, S. Fiebiger, K. Göbel, T. Heftrich, T. Kausch, C. Köppchen, D. Kurtulgil, C. Langer, B. Thomas and M. Weigand, Int. J. Mod. Phys. A **33** 1843011 (2018)
[27] A. Chieffi and M. Limongi, Astrophys. J. **764**, 21 (2013).
[28] P. Hoppe, P. Annen, R. Strebel, R., et al., ApJL **487**, L101 (1997).
[29] M. Pignatari et al., ApJL **767**, L22 (2013).
[30] W. Fujiya, P. Hoppe, E. Zinner, M. Pignatari, and F. Herwig, ApJL **776**, L29 (2013).
[31] P. Hoppe, R. J. Stancliffe, M. Pignatari, and S. Amari ApJ **887**, 1 (2019).
[32] A. L. Sallaska, C. Iliadis, A. E. Champange, S. Goriely, S. Starrfield, and F. X. Timmes, The Astrophys. J., Supplement Series, **207:18**, 1 (2013).
[33] C. Iliadis, A. Champagne, J. José, S. Starrfield and P. Tupper, Astrophys. J. **142**, 105 (2002)
[34] C. Wrede, AIP Advances **4**, 041004 (2014)

TABLE I: Properties of the resonance states for ^{34}S(p,γ)^{35}Cl from 5.8 to 7.2 MeV. $J_i^\pi = 0^+$. Q = 6.371 MeV. n is the number of the level in the spectrum. k is the number of the level for a given J^π value. $C^2S^+ = [(2J_f+1)/(2J_i+1)]$ C^2S.

n	J^π	k	E_x(th)	E_{res}	C^2S^+	Γ_γ	Γ_p	$\omega\gamma$
			(MeV)	(MeV)	$\ell = 0(1)$	(eV)	(eV)	(eV)
2	$1/2^+$	1	1.226		1.9×10^{-1}	1.8×10^{-3}		
9	$1/2^+$	2	3.981		3.8×10^{-2}	2.2×10^{-2}		
10	$3/2^-$	1	4.079		1.1	2.7×10^{-2}		
17	$1/2^+$	3	4.930		2.3×10^{-3}	1.3×10^{-1}		
20	$3/2^-$	2	5.119		1.7×10^{-1}	8.0×10^{-2}		
21	$1/2^-$	1	5.182		3.5×10^{-2}	1.3×10^{-2}		
23	$3/2^-$	3	5.429		3.7×10^{-1}	2.5×10^{-2}		
35	$1/2^-$	2	5.961		1.3×10^{-1}	2.6×10^{-1}		
39	$3/2^-$	4	6.142		2.8×10^{-2}	5.3×10^{-2}		
42	$3/2^-$	5	6.338		7.7×10^{-2}	2.8×10^{-1}		
47	$1/2^-$	3	6.455	0.084	1.2×10^{-1}	1.7×10^{-1}	3.3×10^{-15}	3.3×10^{-15}
49	$3/2^-$	6	6.519	0.148	4.0×10^{-2}	2.1×10^{-1}	3.1×10^{-10}	6.3×10^{-10}
53	$1/2^-$	4	6.703	0.332	1.2×10^{-1}	2.1×10^{-1}	1.3×10^{-3}	1.3×10^{-3}
57	$3/2^-$	7	6.813	0.442	1.4×10^{-1}	1.9×10^{-1}	2.6×10^{-2}	4.6×10^{-2}
63	$3/2^-$	8	7.060	0.689	1.9×10^{-3}	1.3×10^{-1}	3.6×10^{-2}	5.7×10^{-2}
67	$1/2^+$	4	7.112	0.741	1.1×10^{-3}	9.3×10^{-1}	2.3×10^{-1}	1.9×10^{-1}
68	$3/2^-$	9	7.177	0.806	4.0×10^{-4}	2.6×10^{-1}	2.9×10^{-2}	5.3×10^{-2}
70	$1/2^-$	5	7.198	0.827	1.8×10^{-2}	1.9×10^{-1}	3.2	1.8×10^{-1}
72	$1/2^+$	5	7.305	0.934	9.0×10^{-3}	2.0	1.2×10^{1}	1.7
78	$1/2^-$	6	7.415	1.044	1.3×10^{-1}	2.3×10^{-1}	1.4×10^{2}	2.3×10^{-1}

TABLE II: Properties of the resonance states for ^{34g}Cl(p,γ)^{35}Ar from 5.8 to 6.8 MeV. $J_i^\pi = 0^+$. Q = 5.896 MeV. n is the number of the level in the spectrum. k is the number of the level for a given J^π value. $C^2S^+ = [(2J_f+1)/(2J_i+1)]$ C^2S.

n	J^π	k	E_x(th)	E_{res}	C^2S^+	Γ_γ	Γ_p	$\omega\gamma$
			(MeV)	(MeV)	$\ell = 0(1)$	(eV)	(eV)	(eV)
2	$1/2^+$	1	1.226		9.4×10^{-2}	1.0×10^{-3}		
9	$1/2^+$	2	3.981		1.9×10^{-2}	2.5×10^{-2}		
10	$3/2^-$	1	4.079		5.5×10^{-1}	2.7×10^{-2}		
17	$1/2^+$	3	4.930		1.1×10^{-3}	1.1×10^{-1}		
20	$3/2^-$	2	5.119		8.4×10^{-2}	7.9×10^{-2}		
21	$1/2^-$	1	5.182		1.8×10^{-2}	1.3×10^{-2}		
23	$3/2^-$	3	5.429		1.8×10^{-1}	2.5×10^{-2}		
35	$1/2^-$	2	5.961	0.065	6.5×10^{-2}	2.6×10^{-1}	3.6×10^{-20}	3.6×10^{-20}
39	$3/2^-$	4	6.142	0.246	1.4×10^{-2}	4.9×10^{-2}	1.9×10^{-7}	3.8×10^{-7}
42	$3/2^-$	5	6.338	0.442	3.9×10^{-2}	2.8×10^{-1}	2.4×10^{-3}	4.9×10^{-3}
47	$1/2^-$	3	6.455	0.559	6.2×10^{-2}	1.7×10^{-1}	1.2×10^{-1}	7.0×10^{-2}
49	$3/2^-$	6	6.519	0.623	2.0×10^{-2}	2.1×10^{-1}	6.2×10^{-2}	9.5×10^{-2}
53	$1/2^-$	4	6.703	0.807	6.2×10^{-2}	2.0×10^{-1}	4.5	1.9×10^{-1}
57	$3/2^-$	7	6.813	0.917	6.9×10^{-2}	1.9×10^{-1}	7.6	3.7×10^{-1}
63	$3/2^-$	8	7.061	1.165	9.7×10^{-4}	1.3×10^{-1}	6.8×10^{-1}	2.2×10^{-1}

TABLE III: Properties of the resonance states for ^{34m}Cl(p,γ)^{35}Ar from 5.8 to 6.8 MeV. $J^\pi_i = 3^+$. Q = 6.042 MeV. n is the number of the level in the spectrum. k is the number of the level for a given J^π value. $C^2S^+ = [(2J_f+1)/(2J_i+1)]\ C^2S$.

n	J^π	k	E_x(th)	E_{res}	C^2S^+	Γ_γ	Γ_p	$\omega\gamma$
			(MeV)	(MeV)	$\ell = 0(1)$	(eV)	(eV)	(eV)
31	$5/2^-$	3	5.823		4.8×10^{-3}	1.7×10^{-1}		
32	$5/2^+$	5	5.836		5.4×10^{-2}	5.6×10^{-2}		
33	$7/2^-$	4	5.871		5.3×10^{-2}	2.8×10^{-2}		
34	$9/2^-$	3	5.928		1.6×10^{-3}	1.9×10^{-3}		
37	$5/2^-$	4	6.048		3.8×10^{-3}	6.8×10^{-2}		
38	$7/2^-$	5	6.113	0.071	5.3×10^{-2}	4.6×10^{-2}	8.5×10^{-19}	4.9×10^{-19}
39	$3/2^-$	4	6.142	0.100	6.1×10^{-3}	4.9×10^{-2}	3.4×10^{-15}	9.7×10^{-16}
40	$9/2^-$	4	6.216	0.174	1.6×10^{-3}	6.8×10^{-3}	1.4×10^{-10}	9.7×10^{-11}
41	$5/2^-$	5	6.244	0.202	1.9×10^{-2}	8.9×10^{-2}	3.9×10^{-8}	1.7×10^{-8}
42	$3/2^-$	5	6.338	0.296	6.2×10^{-3}	2.8×10^{-1}	1.1×10^{-5}	3.2×10^{-6}
43	$7/2^+$	4	6.377	0.335	2.8×10^{-2}	6.3×10^{-2}	5.1×10^{-4}	2.9×10^{-4}
44	$5/2^-$	6	6.401	0.359	6.6×10^{-5}	5.4×10^{-2}	1.5×10^{-6}	6.6×10^{-7}
45	$5/2^+$	6	6.415	0.373	3.2×10^{-4}	8.1×10^{-1}	3.5×10^{-5}	1.5×10^{-5}
46	$7/2^-$	6	6.445	0.403	1.9×10^{-5}	4.8×10^{-2}	2.7×10^{-6}	1.5×10^{-6}
48	$7/2^-$	7	6.518	0.476	1.7×10^{-1}	4.3×10^{-2}	9.5×10^{-2}	1.7×10^{-2}
49	$3/2^-$	6	6.519	0.477	8.1×10^{-2}	2.1×10^{-1}	9.0×10^{-2}	1.8×10^{-2}
50	$7/2^-$	8	6.598	0.556	2.8×10^{-2}	7.7×10^{-2}	9.0×10^{-2}	2.4×10^{-2}
51	$5/2^-$	7	6.687	0.645	2.3×10^{-1}	3.7×10^{-1}	4.6	1.5×10^{-1}
55	$5/2^-$	8	6.749	0.707	2.6×10^{-2}	1.4×10^{-1}	1.3	5.4×10^{-2}
56	$9/2^-$	5	6.805	0.763	2.3×10^{-1}	1.7×10^{-2}	1.4×10^{1}	1.2×10^{-2}